Supporting Information

Gate-Tunable Transmissive Metasurfaces with Dual-Resonance-Enhanced Modulation

*Sota Ito[1, †], Soh Uenoyama[1, †, *], Ruzan Sokhoyan[2, †], Jared Sisler[2], and Harry A. Atwater[2, *]*

AUTHOR ADDRESS

1: Central Research Laboratory, Hamamatsu Photonics K.K., 5000 Hirakuchi, Hamana-ward, Hamamatsu City 434-8601, Japan, E-mail: so.uenoyama@crl.hpk.co.jp,

2: Thomas J. Watson Laboratories of Applied Physics, California Institute of Technology, Pasadena, CA, 91125, USA, E-mail: haa@caltech.edu.

† S.I., S.U., and R.S. contributed equally to this work.

S1: Transmission map of the full a-Si thickness (t = 0 – 800 nm)

Figure S1 (a, b) shows the full transmission map as a function of the incident wavelength (λ = 1000–1700 nm) and the Si layer thickness (t_{Si} = 0–800 nm) with and without the Au nano-antenna, respectively. Partial simulation results (t_{Si} = 0–400 nm) are presented in Figure 2b of the main manuscript. As the thickness of the Si layer increases, multiple Fabry–Pérot (FP) modes emerge. In these simulations, a SiO_2 substrate was included, and the plane-wave light source was located within the SiO_2 substrate, illuminating the structure along the positive z-direction. The SiO_2 substrate was extended into the perfectly matched layer (PML) boundary.

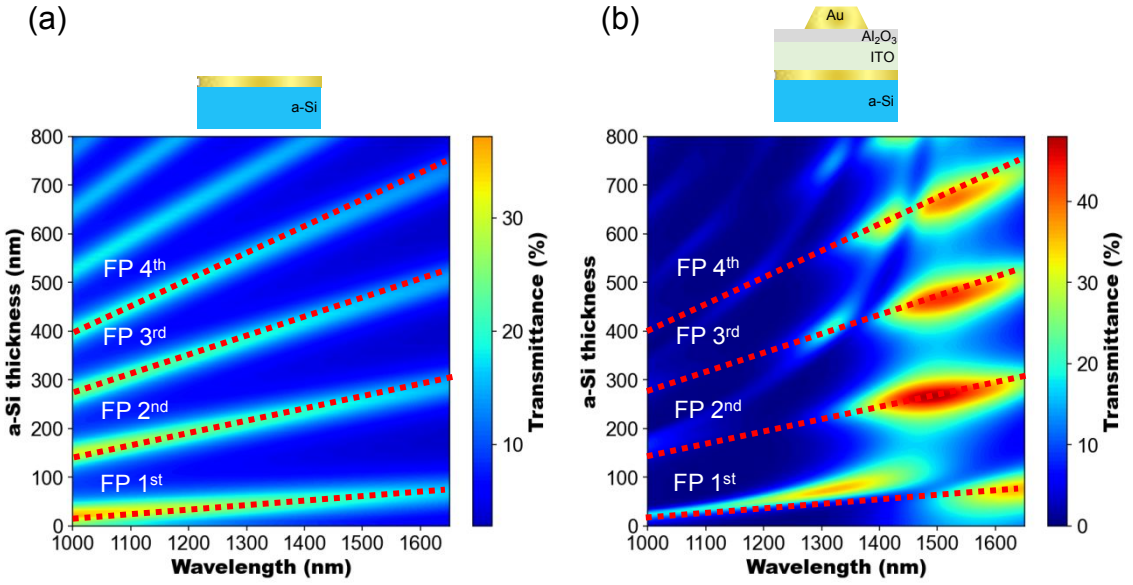


Figure S1. (a, b) Transmission map as a function of incident wavelength (λ = 1000 – 1700 nm). and Si layer thickness (t = 0 – 800 nm) with and without the Au nano-antenna, respectively. The assumed geometric parameters are the same as in Fig. 2 of the main manuscript.

S2: Transmittance spectra with and without the nano-antenna

Figure S2 shows the transmittance spectra as a function of wavelength for the cases with (red line) and without (black line) the Au nano-antenna. As shown in Figure S2, the transmittance is significantly enhanced when the nano-antenna is present. This enhancement indicates that the nano-antenna facilitates efficient coupling between the underlying resonant mode of the planar heterostructure and free-space radiation on the transmission side.

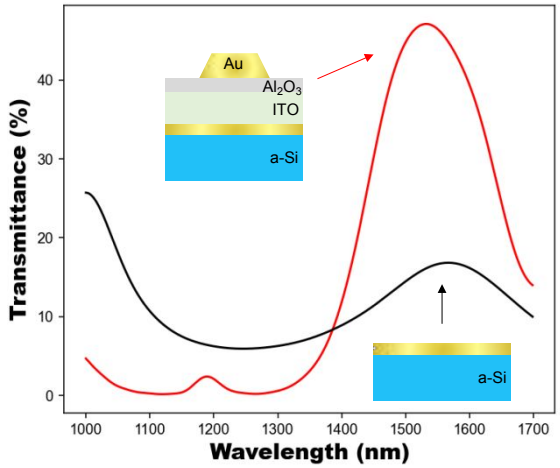


Figure S2. Transmission spectra with and without the Au nano-antenna. The red and black lines correspond to the cases with and without the nano-antenna, respectively. The assumed geometric parameters are the same as in Fig. 2 of the main manuscript. The thickness of the a-Si layer is 275 nm.

S3: Guided-Mode Resonance (GMR) Revealed by Period Sweep

Figure S3a shows the configuration of the Au nano-antenna. Figure S3b shows the transmittance spectra as a function of wavelength for different grating periods. The additional mode excitation observed ranges from $1100 - 1250$ nm for the case of t_{Si} = 275 nm originates from a guided-mode resonance (GMR) in the Si layer. At a representative wavelength of 1180 nm, the structural period (P) of 400 nm becomes larger than the effective wavelength inside silicon. Considering the refractive index of Si (n_{Si} ≈ 3.6 at 1180 nm), the effective wavelength in the Si layer is approximately 1180 / 3.6 ≈ 328 nm, which is smaller than the lattice period. Under this condition, diffraction occurs and provides the required momentum matching to couple the incident light into a guided mode supported by the Si slab. The guided-mode resonance is excited via the grating period, following the momentum matching condition. For normal incidence, the resonance wavelength is given by $\lambda_{GM} = P \times n_{eff}$. To confirm the origin of this mode, we swept the structural period and analyzed the transmittance spectra. The observed peak shifts linearly with the period, as shown in Figure S3c, which is consistent with the guided-mode resonance condition. Therefore, this resonance is attributed to a guided-mode resonance rather than to a localized plasmonic resonance of the Au nanoantenna.

Figure S3d shows a schematic configuration illustrating the behavior of the Au nanoantenna around λ ≈ 1500 nm, where a hybrid mode formed by the Fabry–Pérot (FP) mode and the gap plasmon (GP) mode is excited. Figure S3e presents the corresponding transmittance spectra, while Figure S3f plots the transmission peak wavelength as a function of the structural period. In contrast to the GMR, this peak exhibits negligible dependence on the grating period, indicating that it originates from a localized plasmonic

mode confined within the nanoantenna gap, rather than from a grating-assisted diffractive resonance.

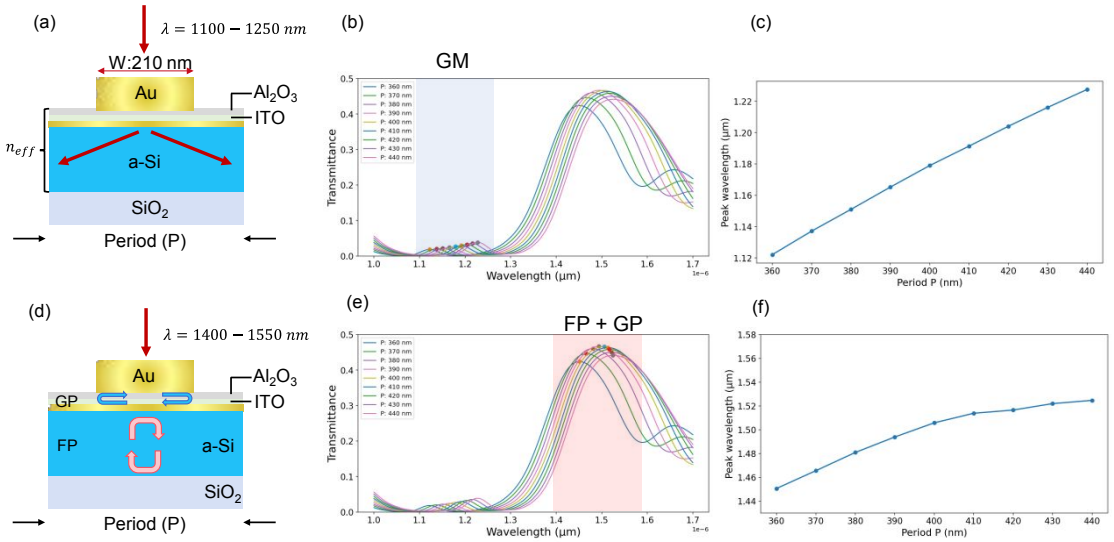


Figure S3. Transmittance characteristics for different grating periods.

(a) Configuration of the Au nano-antenna. (b) Transmittance spectra as a function of wavelength for different grating periods. (c) GMR resonance peak wavelength as a function of the grating period. (d) Schematic configuration illustrating the behavior of the Au nanoantenna at λ = 1500 nm. (e) Transmittance spectra showing the Fabry–Pérot (FP) and gap plasmon (GP) modes. (f) FP and GP resonance peak wavelengths as a function of the grating period.

S4: Simulated electric-field intensity distribution with and without the a-Si layer.

Figure S4(a,b) show the electric-field intensity profiles with and without the a-Si layer, respectively. As shown in Figure S4, the presence of the a-Si layer facilitates strong confinement of the incident light within the dielectric layer sandwiched between the top and bottom Au layers.

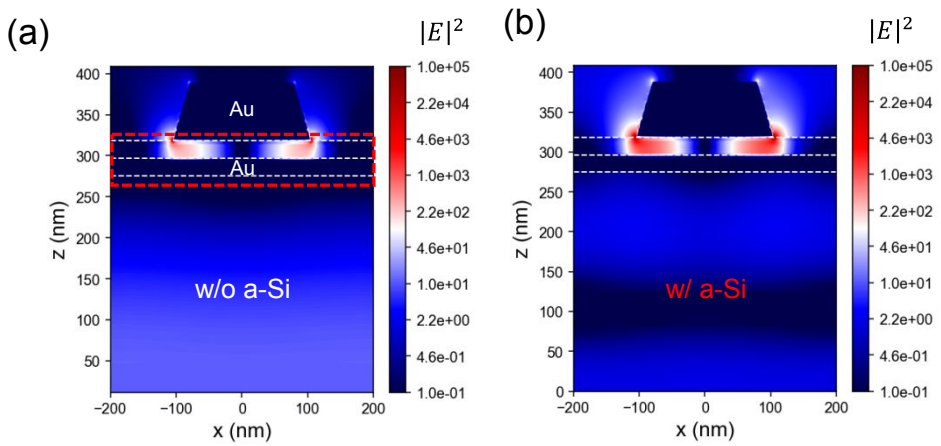


Figure S4. Electric-field intensity distributions.

(a, b) Electric-field intensity distributions with and without the a-Si layer, respectively. The assumed geometric parameters are the same as in Fig. 2 (d)-(e) of the main manuscript.

S5: Transmittance with a semi-transparent Au thin layer

Figure S5 shows the transmittance spectra for different thicknesses of the Au thin layer placed between the ITO layer and the a-Si layer. The Au thin layer plays a critical role in enabling the coupling between the Fabry–Pérot (FP) mode and the gap plasmon mode. However, as the thickness of the Au thin layer increases, optical loss becomes more significant, resulting in a degradation of the transmittance.

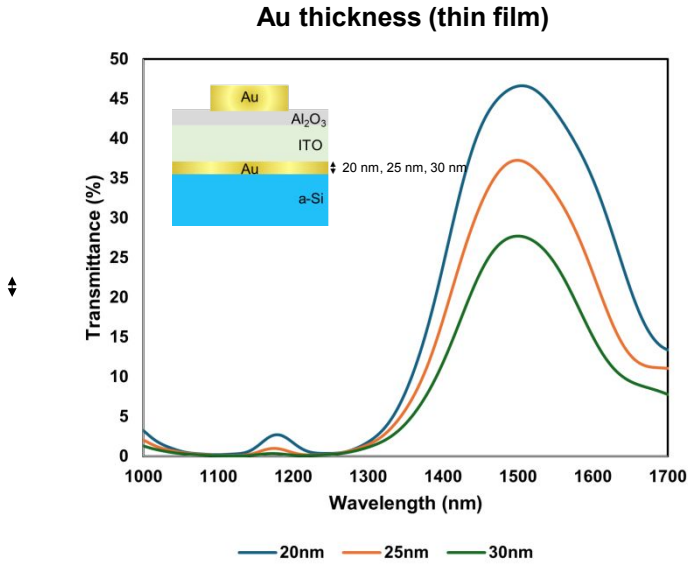


Figure S5. Transmittance spectra of the structure with an Au thin layer for different Au thicknesses of 20, 25, and 30 nm.

S6: Permittivity (real and image part) of the ITO with and without biasing

Figures S6 (Left) and S6 (Right) show the permittivity of the ITO as a function of wavelength, where the real part (left axis) and the imaginary part (right axis) are plotted for different carrier densities N at the same electron mobility μ, corresponding to the cases without ($N = 2.66 \times 10^{20} cm^{-3}$, $\mu = 25.4\ cm^2 V^{-1} s^{-1}, V = 0$ V) and with an applied voltage ($N = 6.00 \times 10^{20} cm^{-3}$, $\mu = 25.4\ cm^2 V^{-1} s^{-1}, V = 3.5$ V). The permittivity of ITO is described using the Drude model. The Drude model is expressed as

$$\varepsilon_{ITO} = \varepsilon_\infty - \frac{{\omega_P}^2}{\omega^2 + i\omega\Gamma}$$

where ε_∞ is the high-frequency permittivity, Γ is the damping constant, and ω is the angular frequency. The plasma frequency ω_p depends on the carrier density N and the electron effective mass m^* as

$$\omega_P{}^2 = \frac{Ne^2}{\varepsilon_0 m^*}$$

Here, ε_0 is the vacuum permittivity, e is the electron charge. The region where the real part of the permittivity satisfies $-1 < \varepsilon < 1$ corresponds to the epsilon-near-zero (ENZ) regime, which is highlighted in green in Figure S3. This ENZ regime is known to strongly modify the optical response owing to pronounced electric-field enhancement

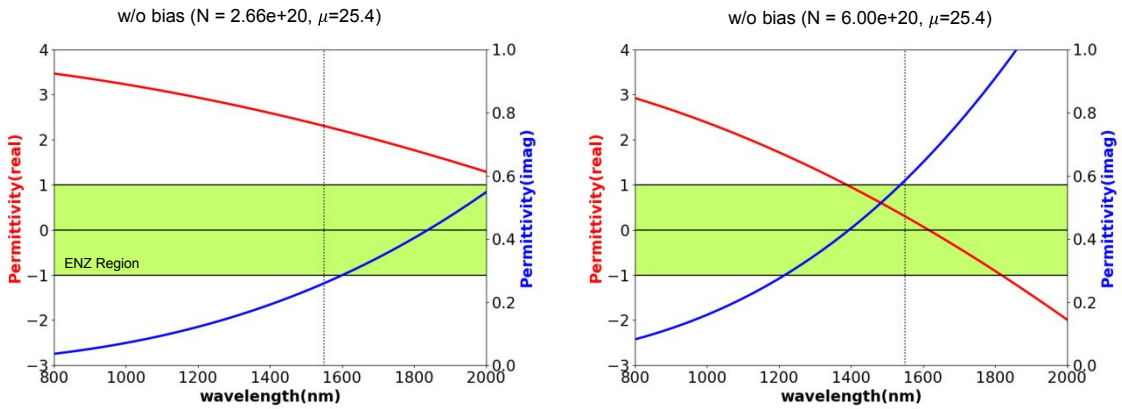


Figure S6. ITO permittivity with ($V = 3.5$ V) and without ($V = 0$ V) the biasing

S7: Experimental Set-up for high-speed modulation

The experimental setup for transmissive modulation measurement, high-speed modulation is shown in Figure S7a and S7b.

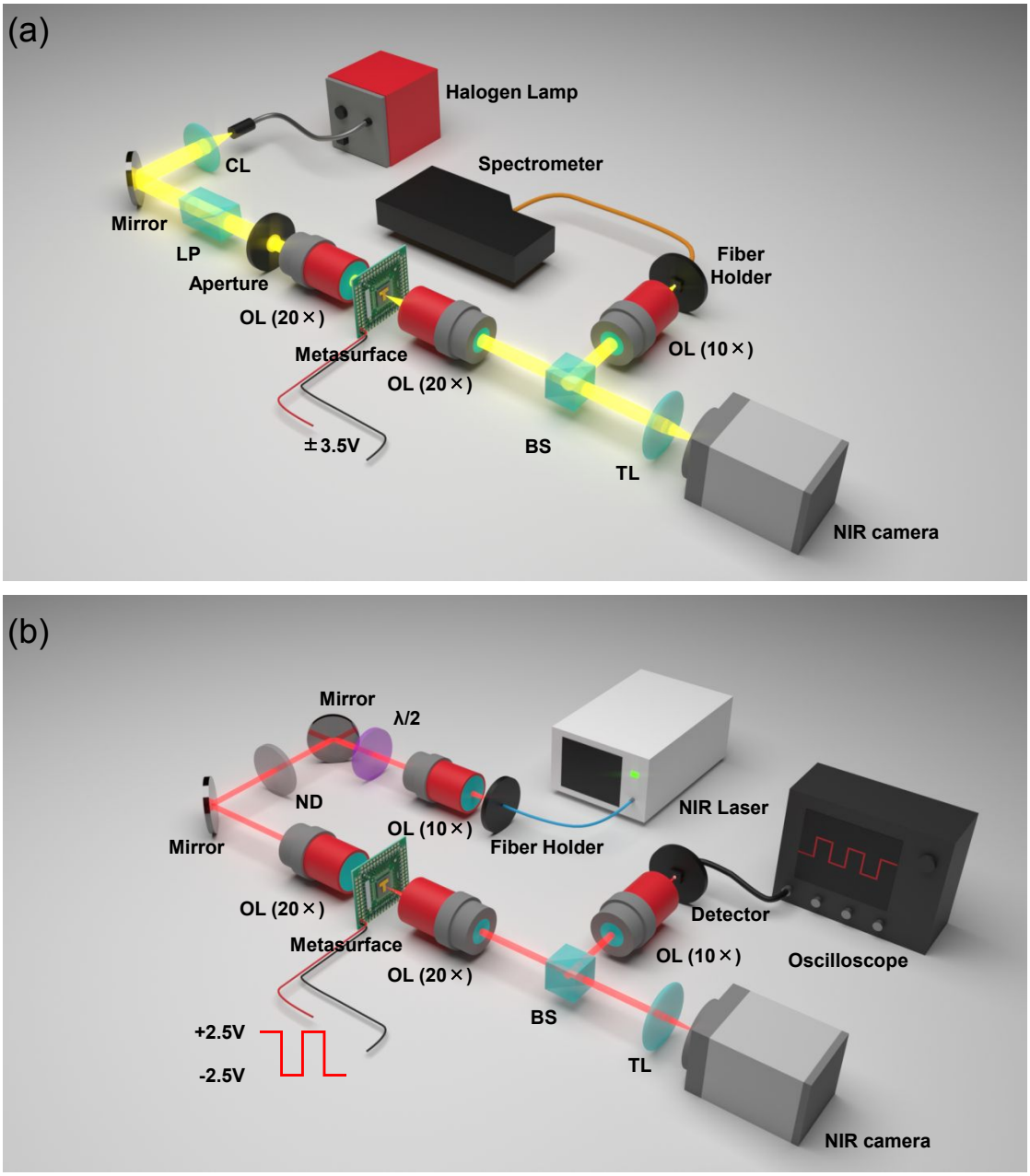


Figure S7. Experimental setup (a) Transmissive modulation measurement, (b) high-speed modulation ND: neutral density filter; TL: tube lens; OL: objective lens; BS: beam splitter; LP: linear polarizer; NIR: Near-infrared.

S8: Simulation model (for CHARGE simulation)

CHARGE simulations were conducted using FDTD (Lumerical Multiphysics) to obtain the carrier concentration profile of the ITO layer during applying the voltage.

The simulation model consists of four layers: the gate (Au nano-antenna, thickness = 100 nm), dielectric (Al_2O_3, 5 nm), semiconductor (ITO, 20 nm), and body (Au bottom mirror, 80 nm). The simulation domain spans from x = −200 nm to 200 nm and z = 0 nm to 205 nm. A voltage bias was applied between the gate and the body.

A monitor was placed within the ITO layer to observe the carrier concentration as a function of the distance from the ITO/Al_2O_3 interface, up to a maximum of 4 nm. The ITO layer was divided into 41 mesh layers, each with a thickness of 0.1 nm, and the minimum mesh size used in the simulation was 0.025 nm.

The carrier concentration in each mesh layer was obtained by solving both the Poisson equation and the carrier diffusion equation. The initial carrier concentration of the ITO was uniformly set to 3.0×10^{20} cm^{-3}. The applied voltages were 0 V for the body and 0–5 V for the gate with a step of 0.1 V. At each voltage step, the carrier concentration profile of the ITO layer was obtained. These results were then converted into permittivity values using the Drude model, which were applied in the FDTD simulation to analyze the voltage-dependent behavior of optical transmittance.

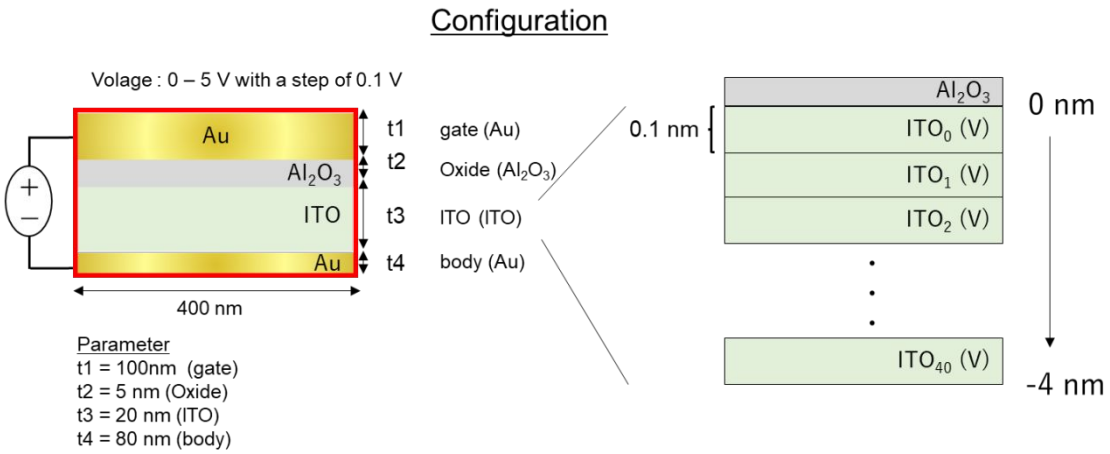


Figure S8. CHARGE simulation configuration